2007 IEEE International Conference on
Robotics and Automation
Roma, Italy, 10-14 April 2007

Design and Theoretical Evaluation of Micro-Surgical Manipulators for Orbital Manipulation and Intraocular Dexterity

Wei Wei[†], Roger Goldman[†], Nabil Simaan[†♣], Howard Fine*, Stanley Chang*
*Advanced Robotics and Mechanism Applications (ARMA) lab[†] & Department of Ophthalmology**
Columbia University, 500 West 120th street, New York, NY 10027, USA
Email: {ww2161, reg2117, ns2236♣}@columbia.edu, hffine@yahoo.com, sc434@columbia.edu

***Abstract*—This paper addresses the design considerations and dexterity evaluation of a novel hybrid two-armed micro-surgical slave robot equipped with intraocular dexterity devices. A unified framework for the kinematic modeling of this robot is presented while using the kinematic constraints stemming from the constrained motion of the eye. An augmented Jacobian describing the kinematics of the eye and the relative motion of each one of the two Intra-Ocular Dexterity Robots (IODR) is presented. Using this framework, the capabilities of this two-armed robot in performing dexterous intraocular operations are evaluated and compared to a similar robot without intra-ocular dexterity. The Kinematic Conditioning Index (KCI) for the proposed robot is shown to be significant. The results presented show an increase of approximately 33% and 47% in translational and rotational KCI respectively.**

I. Introduction

Dexterty deficiency has been identified as a major obstacle hindering complex manipulation in Minimally Invasive Surgery (MIS) [1]. Hence, a significant number of works have addressed robot-assisted enhancement of distal dexterity in MIS [2-11]. Of these works, few addressed the problem of dexterity enhancement in deep surgical fields [6, 10, 12].

Several works addressed robot-assisted ophthalmic surgery. Grace [13] presented a mini tele-surgical parallel robot for the treatment of retinal venous occlusion in ophthalmic surgery. Das et al. [14] and Charles, et al. [15] developed a precision cable-driven master-and-slave tele-robotic system called RAMS. The system provided tremor filtering, amplified force feedback, and programmable constrained motion of the instrument in the eye to minimize surgical impacts. Ang et al. [16] developed a hand-held microsurgical instrument for vitreoretinal microsurgery via tremor canceling. The instrument tip was attached to a three Degrees of Freedom (DoF) parallel manipulator with piezoelectric actuation and inertial gyroscopic sensors. The actuators moved the tool tip in opposite direction to the tremor, thereby suppressing the erroneous motion. Taylor et al. and Kumar et al. [17, 18] presented a cooperative manipulation robot for microsurgical applications.

All the above mentioned works addressed surgery of the eye while focusing on manipulating straight needles and instruments inside the eye. Ikuta and Kato [19] designed a hand-held forceps with an active joint and fiberscope for providing intra-ocular dexterity and parallel visualization to address the lack of dexterity inside the eye.

In this contribution, we address microsurgery of the eye while considering the overall requirements of a surgical procedure including the precise manipulation of the instrument End Effector (EE), as cited above, and gross manipulation of the eye for access and visualization. Based on these surgical needs, we present a two-armed tele-robotic slave equipped with IODR for high precision control of tools inside the orbit and for precise manipulation of the eyeball under the microscope. We present a unified framework for the kinematic modeling of this two-armed robotic system and quantify the improvement in intra-ocular dexterity when the two-armed robotic slave is used with and without the IODR.

II. Surgical Needs and System Layout

A. Surgical Setup

As depicted in Fig. 1, two surgeons coordinate activities to perform the ophthalmic surgical procedures. The main surgeon sits superior to the patient's head and performs most of the surgical tasks including manipulation of the surgical tools and the light source. The assistant surgeon sits beside the patient's head to provide irrigation and removal of fluids and to adjust the placement of the visualization of the external lenses. There is also another assistant sitting on the other side of the patient for tool delivery to the main surgeon.

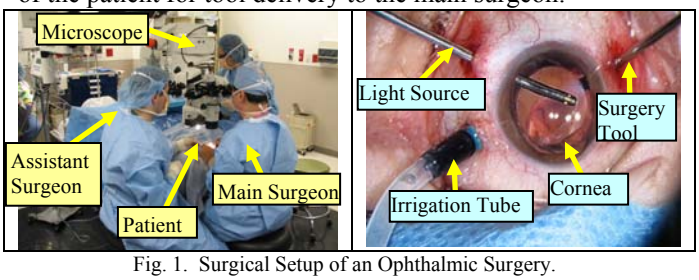

Fig. 1. Surgical Setup of an Ophthalmic Surgery.

Three incisions are typically made in the sclera to provide access to the inner vitreous body for one irrigation tube, one light source and one surgical instrument. The irrigation tube injects liquid to maintain intraocular pressure. The light source illuminates an area on the retina for proper visualization under the microscope. The surgical tools including picks, micro tweezers, vitrectomy cutters and other laser ablation devices [20] vary dependent on the

♣ corresponding author

requirements of the procedure. The surgeons operate using a microscope while visualizing the retina through a dilated iris. Because the visual field does not include the entire retinal surface, the surgery often requires tilting the eye under the microscope in order to view peripheral areas of the retina.

Although previous works addressed major challenges of reduced tremor, high precision, and force feedback in eye surgery, we believe that the surgical need to manipulate several tools and to tilt the eye under the microscope requires a system capable of manipulating instruments inside the eye while stabilizing and/or manipulating the eye under the microscope. This concept of cooperative manipulation of an organ while operating inside the organ is an additional novel element that guides the eventual goal of our work.

B. System Description

To increase the dexterity, precision, and ease of ophthalmic microsurgical procedures, a 16-DoF hybrid robotic system is proposed, Fig. 3. This system will allow high precision dexterous manipulation of surgical instruments within the vitreous body of the eye and macroscopic rotation of the eye for surgical field visibility. A frame is secured without trauma to the patient's head with a locking bite-plate and coronal strap that rigidly affixes the frame to the patient. Two identical hybrid robotic arms are rigidly attached to this frame. Each robotic arm is composed from a 2 DoF IODR and a 6 DoF parallel robot. This design will allow 5 DoFs for the surgical tools inside the eye, as compared to 4 DoF tools used currently. We believe this will be useful in applications requiring fine dexterous manipulation such as Internal Limiting Membrane (ILM) peeling and treatment of severe retinal detachments. The 2 DoF IODR provides intra-ocular dexterity while the parallel robot provides global precise positioning of the eye and the surgical tool inside the eye. The IODR utilizes a pre-shaped NiTi tube that bends in one DoF as it is extended outside of a straight cannula, Fig. 4. This design is similar to the work of [21] and [22]. The cannula of the IODR rotates about its axis to provide the second DoF inside the eye. For the parallel robot, we propose the Stewart-Gough platform design due to its rigidity, compactness, positional accuracy, and high payload-to-weight ratio.

C. Dimensional Synthesis

Dimensional synthesis for each branch of the system was performed based on the following assumptions specified in the literature and by feedback from ophthalmic surgeons:

1) The eyeball is approximated with a spherical model with a radius of 11.5 mm [23].

2) The lower hemisphere of the eyeball is to be reached by the robot EE for retinal surgery.

3) Incision points in the scleral are located on a circle encompassing the pupil and offset 4mm from the pupil.

4) A typical surgical procedure requires the tool to work within an area of ±20º around a target point on the retina. A point $[\theta, \phi]$ on the retina is defined as in Fig. 2.

According to the aforementioned assumptions, dimensional synthesis was performed for both arms in two steps. The first step was to dimensionally synthesize the IODR and the second step was the dimensional synthesis of the Stewart/Gough platform. The bending radius of the pre-shaped inner tube was predetermined as 5mm based on the strain limitations of the NiTi. The length of the IODR cannula was chosen as 60mm. The diameter of the inner tube is 0.55mm; the diameter of the cannula is 0.91mm (the typical diameter of ophthalmic surgical tools is 0.51 mm). The IODR is attached to the parallel robot via an adjustable lockable link, Fig. 3. In addition, there is a lockable adjustable joint connecting the IODR to this rigid link. The adjustable joint is assumed to be equipped with absolute encoders. Using this design, surgeons can initially position the robot and lock the adjustable joints at a given "start" configuration. This approach allows minimizing the required workspace of the parallel robot.

With the assumptions, the lower hemisphere of the eyeball was scanned in a simulation by the robot EE tip, and the corresponding lengths and strokes for the parallel legs were recorded. These simulations included static simulations to calculate the required joint forces and the global dexterity of the robot over the reachable workspace [24]. After initial workspace simulations were performed, we decided to place the parallel robots sideways with respect to the patient to avoid the singularities associated with large tilting angles about the x-y axes of the moving platform (commonly known as Hunt's singularity [25]). Due to space limits, further details of the dimensional synthesis are omitted. Simulations of the complete robotic system are presented in Section IV.

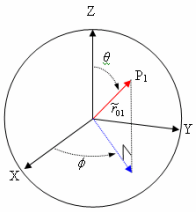

Fig. 2. Definition of a Point on the Retina Based on Euler Angles.

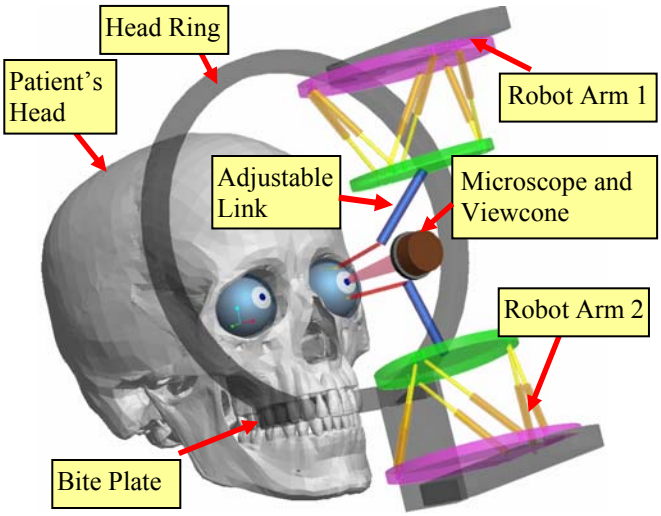

Fig. 3. Model of the Proposed Robotic System.

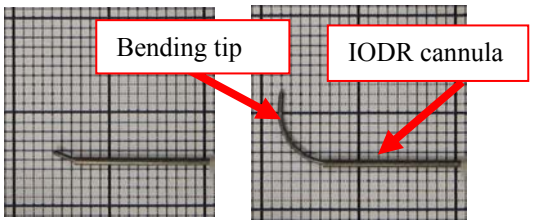

Fig. 4. The IODR Shown in Retracted and Open Configuration.

The final obtained dimensions of the parallel robot are:

1) Radius of the moving platform is 30mm, and radius of the base is 42mm.
2) Separation angle of the moving platform, defined as the angle between two adjacent connection points with respect to the center, is 20º and separation angle of the base is 40º.
3) The required leg dimensions and strokes are shown in Table I.
4) The length of the parallel robot adjustable link is 40mm.

Since the two robotic arms are identical, the above dimensions are also applicable to the second arm. During a surgical procedure, the two arms are expected to have coordinated path planning to perform a surgical task.

TABLE I
LEG DIMENSIONS FOR THE PARALLEL ROBOT.

Leg number	1	2	3	4	5	6
Min length (mm)	66	74	65	61	68	63
Max length (mm)	100	95	105	102	95	100
Stroke (mm)	34	21	40	41	27	37

III. KINEMATIC MODELING

This section presents a unified kinematic model that accounts for the relationship between the joint speeds of the two-armed robot of Fig. 3 and the twist* of the eye and the surgical tools inside the eye.

A. Kinematic Nomenclature

Fig. 5 depicts the eye and the ith hybrid robot. The eye system is enlarged for a clearer view of the EE and the eye coordinate frames. The following coordinate systems are defined to assist in the derivation of the system kinematics. The *world coordinate system {W}* is centered at an arbitrarily predetermined point in the patient's forehead with the patient in a supine position. The $\hat{\mathbf{z}}_W$ axis points vertically and $\hat{\mathbf{y}}_W$ axis points superiorly. The *Stewart base coordinate system* $\{B_i\}$ of the ith hybrid robot is located at point b_i (the center of the base platform) such that the $\hat{\mathbf{z}}_{B_i}$ axis lies perpendicular to the base of the Stewart platform and the $\hat{\mathbf{x}}_{B_i}$ axis lies parallel to $\hat{\mathbf{z}}_W$. The *moving platform coordinate system of the ith hybrid robot* $\{P_i\}$ lies in center of the moving platform, at point p_i, such that the axes lie parallel to $\{B_i\}$ when the Stewart platform lies in a home configuration. The *Stewart extension arm coordinate system of the ith hybrid* $\{Q_i\}$ is attached to the distal end of the arm at point q_i, with $\hat{\mathbf{z}}_{Q_i}$ lying along the direction of the insertion needle of the robot $\overrightarrow{q_i n_i}$, and $\hat{\mathbf{x}}_{Q_i}$ fixed during setup of the vitrectomy procedure. The *IODR base coordinate system of the ith hybrid robot* $\{N_i\}$ lies at point n_i with the $\hat{\mathbf{z}}_{N_i}$ axis also pointing along the insertion needle length $\overrightarrow{q_i n_i}$ and the $\hat{\mathbf{y}}_{N_i}$ axis rotated from $\hat{\mathbf{y}}_{Q_i}$ an angle $q_{s_i 1}$ about $\hat{\mathbf{z}}_{N_i}$. The *EE coordinate system* $\{G_i\}$ lies at point g_i with the $\hat{\mathbf{z}}_{G_i}$ axis pointing in the direction of the EE gripper and the $\hat{\mathbf{y}}_{G_i}$ axis parallel to the $\hat{\mathbf{y}}_{N_i}$ axis. The *eye coordinate system* $\{E\}$ sits at the center point e of the eye with axes parallel to $\{W\}$ when the eye is unactuated by the robot.

The notations used in this paper are defined below:

$i = 1,2$ - index referring to one of the two arms in Fig. 1.

$\{A\}$- An arbitrary right handed coordinate frame with $\{\hat{\mathbf{x}}_A, \hat{\mathbf{y}}_A, \hat{\mathbf{z}}_A\}$ as its associated unit vectors and point a as the location of its origin.

$\mathbf{v}^C_{A/B}, \boldsymbol{\omega}^C_{A/B}$ - Relative linear and angular velocities of frame $\{A\}$ with respect to frame $\{B\}$, expressed in frame $\{C\}$. Unless specifically stated, all vectors in this work are expressed in $\{W\}$.

$\mathbf{v}_A, \boldsymbol{\omega}_A$ - Absolute linear and angular velocities of frame $\{A\}$

${}^A\mathbf{R}_B$ - Rotation matrix of the moving frame $\{B\}$ with respect to the frame $\{A\}$.

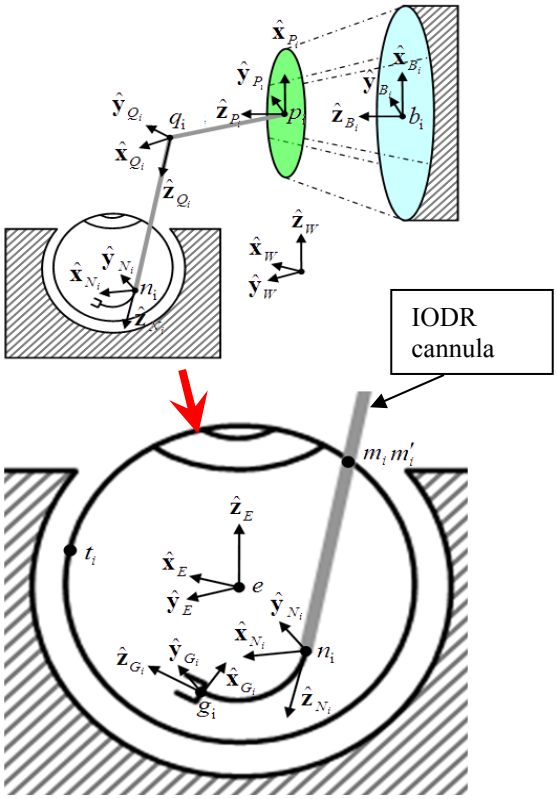

Fig. 5. Kinematic Model of the Eye and ith Hybrid Robot.

$\mathrm{Rot}(\hat{\mathbf{x}}_A, \alpha)$- Rotation matrix about unit vector $\hat{\mathbf{x}}_A$ by angle α.

* In this paper we use the term twist to indicate the 6-dimensional vector of linear velocity and angular velocity where the linear velocity is given by the first three components. This definition is different from the standard nomenclature where the angular velocity precedes the linear velocity.

$[\mathbf{b}\times]$- Skew symmetric cross product matrix of $\mathbf{b}$.

$\dot{\mathbf{q}}_{P_i} = [\dot{q}_{P_i1}, \dot{q}_{P_i2}, \dot{q}_{P_i3}, \dot{q}_{P_i4}, \dot{q}_{P_i5}, \dot{q}_{P_i6}]^t$ -The active joint speeds of the i[th] Stewart platform.

$\dot{\mathbf{q}}_{s_i} = [\dot{q}_{s_i1}, \dot{q}_{s_i2}]^t$ - Joint speeds of the IODR. The first component is the rotation speed about the axis of the IODR cannula, Fig. 5, and the second component is the bending angular rate of the pre-shaped tube, Fig. 4.

$\dot{\mathbf{x}}_A = [\dot{x}_A, \dot{y}_A, \dot{z}_A, \omega_{Ax}, \omega_{Ay}, \omega_{Az}]^t$ - Twist of frame *{A}*.

$\dot{\mathbf{x}}_{P_i} = [\dot{x}_{P_i}, \dot{y}_{P_i}, \dot{z}_{P_i}, \omega_{P_ix}, \omega_{P_iy}, \omega_{P_iz}]^t$ - Twist of the i[th] moving Stewart platform.

$\dot{\mathbf{x}}_{n_i}$ -Twist of the i[th] insertion needle end/base of snake.

$\dot{\mathbf{x}}_e$ -Angular velocity of the eye.

$^A\overrightarrow{ab}$ -Vector from point *a* to *b* expressed in frame *{A}*.

r - Bending radius of the pre-curved tube.

$\mathbf{W}(\vec{a}) = \begin{bmatrix} \mathbf{I}_{3\times3} & [-(\vec{a})\times] \\ \mathbf{0}_{3\times3} & \mathbf{I}_{3\times3} \end{bmatrix}$ - Twist transformation operator. This operator is defined as a function of the translation of the origin of the coordinate system indicated by vector $\vec{a}$. $\mathbf{W}$ is a 6x6 upper triangular matrix with the diagonal elements being unity and the upper right block being a cross product matrix [26].

B. Kinematic Relations

The kinematic modeling of the system has to include the kinematic constraints due to the incision points in the eye and the limited DoF of the eye. In the following section we present the kinematics of the two-armed robot with the eye while describing the relative kinematics of the IODR end effector with respect to a target point on the retina.

1) Hybrid Robot: The Jacobian of the Stewart/Gough platform, relating the twist of the moving platform frame *{P_i}* to the joint parameters $\dot{\mathbf{q}}_{P_i}$, is given by [27] .

$$\mathbf{J}_{P_i}\dot{\mathbf{x}}_{P_i} = \dot{\mathbf{q}}_{P_i} \tag{1}$$

To develop the next step in the kinematic chain of the i[th] hybrid robot, to *{Q_i}*, the linear and angular velocities are expressed w.r.t respective velocities of the moving platform:

$$\mathbf{v}_{Q_i} = \mathbf{v}_{P_i} + \boldsymbol{\omega}_{P_i} \times (\overrightarrow{p_iq_i}) \tag{2}$$

$$\boldsymbol{\omega}_{Q_i} = \boldsymbol{\omega}_{P_i} \tag{3}$$

Writing Eqs. (2) and (3) in matrix form results in the twist of the distal end of the adjustable lockable link:

$$\dot{\mathbf{x}}_{Q_i} = \mathbf{A}_i\dot{\mathbf{x}}_{P_i} \tag{4}$$

where $\mathbf{A}_i = \mathbf{W}(\overrightarrow{p_iq_i})$, is the twist transformation matrix defined in subsection III.A.

The kinematic relationship of the frame *{N_i}* can be similarly related to by combining the linear and angular velocities. The linear and angular velocities are:

$$\mathbf{v}_{N_i} = \mathbf{v}_{Q_i} + \boldsymbol{\omega}_{Q_i} \times (\overrightarrow{q_in_i}) \tag{5}$$

$$\boldsymbol{\omega}_{N_i} = \boldsymbol{\omega}_{Q_i} + \dot{q}_{s_i1}\hat{\mathbf{z}}_{Q_i} \tag{6}$$

Eqs. (5) and (6) expressed in matrix form yield:

$$\dot{\mathbf{x}}_{N_i} = \mathbf{B}_i\dot{\mathbf{x}}_{Q_i} + \begin{bmatrix} \mathbf{0} \\ \hat{\mathbf{z}}_{Q_i} \end{bmatrix}\dot{q}_{s_i1} \tag{7}$$

where $\mathbf{B}_i = \mathbf{W}(\overrightarrow{q_in_i})$.

Continuing to the final serial frame in the hybrid robot, *{G_i}*, the linear and angular velocities can be written as

$$\mathbf{v}_{G_i} = \mathbf{v}_{N_i} + \dot{q}_{s_i2}\mathrm{r}\hat{\mathbf{z}}_{G_i} + \boldsymbol{\omega}_{N_i} \times (\overrightarrow{n_ig_i}) \tag{8}$$

$$\boldsymbol{\omega}_{G_i} = \boldsymbol{\omega}_{N_i} + \dot{q}_{s_i2}\hat{\mathbf{y}}_{N_i} \tag{9}$$

Eqs. (8) and (9) expressed in matrix form yield:

$$\dot{\mathbf{x}}_{G_i} = \mathbf{C}_i\dot{\mathbf{x}}_{N_i} + \begin{bmatrix} \mathrm{r}\hat{\mathbf{z}}_{G_i} \\ \hat{\mathbf{y}}_{N_i} \end{bmatrix}\dot{q}_{s_i2} \tag{10}$$

where $\mathbf{C}_i = \mathbf{W}(\overrightarrow{n_ig_i})$.

To express the kinematics of the frame of the robot EE, *{G_i}*, as a function of the joint parameters of the i[th] hybrid robotic system, the serial relationships developed above are combined. Beginning with the relationship between the twist of frame *{G_i}* and *{N_i}* (10) and inserting the relationship between *{N_i}* and *{Q_i}* (7) yields:

$$\dot{\mathbf{x}}_{G_i} = \mathbf{C}_i\mathbf{B}_i\dot{\mathbf{x}}_{Q_i} + \mathbf{C}_i\begin{bmatrix} \mathbf{0} \\ \hat{\mathbf{z}}_{Q_i} \end{bmatrix}\dot{q}_{s_i1} + \begin{bmatrix} \mathrm{r}\hat{\mathbf{z}}_{G_i} \\ \hat{\mathbf{y}}_{N_i} \end{bmatrix}\dot{q}_{s_i2} \tag{11}$$

By reintroducing the matrix $\mathbf{C}_i$ to the $\dot{q}_{s_i1}$ term, the serial joints of the hybrid system can be parameterized as follows:

$$\dot{\mathbf{x}}_{G_i} = \mathbf{C}_i\mathbf{B}_i\dot{\mathbf{x}}_{Q_i} + \mathbf{J}_{s_s}\dot{\mathbf{q}}_{s_i} \tag{12}$$

where $\mathbf{J}_{s_i} = \begin{bmatrix} [(-\overrightarrow{n_ig_i})\times]\hat{\mathbf{z}}_{Q_i} & \mathrm{r}\hat{\mathbf{z}}_{G_i} \\ \hat{\mathbf{z}}_{Q_i} & \hat{\mathbf{y}}_{N_i} \end{bmatrix}$ represents the Jacobian of the IODR including the speeds of rotation about the axis of the IODR cannula and the bending of the pre-curved cannula.

Inserting the relationship between *{Q_i}* and *{P_i}* (4) and the inverse of the Stewart Jacobian equation (1) and condensing terms yields the final Jacobian for the i[th] hybrid robot:

$$\dot{\mathbf{x}}_{G_i} = \mathbf{J}_{h_i}\dot{\mathbf{q}}_{h_i} \tag{13}$$

where $\mathbf{J}_{h_i} = \left[\mathbf{C}_i\mathbf{B}_i\mathbf{A}_i\mathbf{J}_{P_i}^{-1}\ ,\ \mathbf{J}_{s_i}\right]$.

2) Eye: The eye is modeled as a rigid body constrained to spherical motion by the geometry of the orbit and musculature. Roll-Pitch-Yaw angles are chosen to describe the orientation such that the rotation matrix specifying the eye frame *{E}* with respect to *{W}* is $^W\mathbf{R}_e = \mathbf{R}_z\mathbf{R}_y\mathbf{R}_x$ where $\mathbf{R}_x = \mathrm{Rot}(\hat{\mathbf{x}}_W, \alpha)$, $\mathbf{R}_y = \mathrm{Rot}(\hat{\mathbf{y}}_W, \beta)$, and $\mathbf{R}_z = \mathrm{Rot}(\hat{\mathbf{z}}_W, \gamma)$.

The desired angular velocity of the eye can therefore be parameterized by:

$$\dot{\mathbf{x}}_e = [\dot{\alpha}, \dot{\beta}, \dot{\gamma}]^t \tag{14}$$

3) Modeling of the kinematics of the End Effector (EE) with respect to the eye: With the kinematics of the eye and the i[th] hybrid robotic system characterized separately, the formulations can be combined to define the kinematic structure of the eye and i[th] hybrid robot. This relationship allows expression of the robot joint parameters based on the desired velocity of the EE with respect to the eye and the desired angular velocity of the eye. To achieve this

relationship, an arbitrary goal point on the retinal surface t_i is chosen, Fig. 5. The angular velocity of the eye (14) imparts a velocity at point t_i :

$$\mathbf{v}_{t_i} = \mathbf{T}_i \dot{\mathbf{x}}_e \tag{15}$$

where $\mathbf{T}_i = \left[(-\overrightarrow{et_i})\times\right]$.

The linear velocity of the EE frame of the robot with respect to the goal point t_i can be written as:

$$\mathbf{v}_{g_i/t_i} = \mathbf{v}_{g_i} - \mathbf{v}_{t_i} \tag{16}$$

Inserting (13) and (15) into (16) yields a linear velocity of the EE as a function of the robot joint parameters and the desired eye velocity:

$$\mathbf{v}_{g_i/t_i} = [\mathbf{I}_{3\times3}, \mathbf{0}_{3\times3}]\mathbf{J}_{h_i}\dot{\mathbf{q}}_{h_i} - \mathbf{T}_i\dot{\mathbf{x}}_e \tag{17}$$

Similarly, the angular velocity of the EE frame of the robot with respect to the eye frame is:

$$\boldsymbol{\omega}_{g_i/e} = \boldsymbol{\omega}_{g_i} - \boldsymbol{\omega}_e \tag{18}$$

or, by inserting (13) and (15) into (18),

$$\boldsymbol{\omega}_{g_i/e} = [\mathbf{0}_{3\times3}, \mathbf{I}_{3\times3}]\mathbf{J}_{h_i}\dot{\mathbf{q}}_{h_i} - \dot{\mathbf{x}}_e \tag{19}$$

Combining the linear (17) and angular (19) velocities yields the twist of the EE with respect to point t_i .

$$\dot{\mathbf{x}}_{g_i/t_i} = \mathbf{J}_{h_i}\dot{\mathbf{q}}_{h_i} - \mathbf{D}_i\dot{\mathbf{x}}_e \tag{20}$$

where $\mathbf{D}_i = [\mathbf{T}_i, \mathbf{I}_{3\times3}]^t$.

4) Euler Parameterization: The mechanical structure of the hybrid robot in the vitreous cavity allows only 5 DoFs as independent rotation about the $\hat{\mathbf{z}}_{G_i}$ axis is unachievable. This rotation is represented by the third w-v-w Euler angle φ_i [27]. Note, the first angle ϕ_i represents the rotation between the projection of the $\hat{\mathbf{z}}_{G_i}$ axis on the $\hat{\mathbf{x}}_W\hat{\mathbf{y}}_W$ plane and $\hat{\mathbf{x}}_W$ and the second angle θ_i represents rotation between $\hat{\mathbf{z}}_W$ and $\hat{\mathbf{z}}_{G_i}$.

For the purposes of path planning and control, the twist of the system can therefore be parameterized with w-v-w Euler angles and the third Euler angle eliminated by a degenerate matrix $\mathbf{K}_i$, defined in the Appendix, as follows:

$$\tilde{\dot{\mathbf{x}}}_{g_i/t_i} = \mathbf{K}_i\dot{\mathbf{x}}_{g_i/t_i} \tag{21}$$

Inserting this new parameterization into the EE twist (20) yields a relation between the achievable independent velocities and the joint parameters of the hybrid system.

$$\tilde{\dot{\mathbf{x}}}_{g_i/t_i} + \mathbf{K}_i\mathbf{D}_i\dot{\mathbf{x}}_e = \mathbf{K}_i\mathbf{J}_{h_i}\dot{\mathbf{q}}_{h_i} \tag{22}$$

5) Overall Eye-Robot System: The robotic system must be constrained such that the hybrid robots move in concert to control the eye without injuring the structure by tearing the insertion points. This motion is achieved by allowing each insertion arm to move at the insertion point only with the velocity equal to the eye surface at that point, plus any velocity along the insertion needle. This combined motion will constrain the insertion needle to the insertion point without damage to the structure.

To assist in the development of this constraint, point m_i is defined at the insertion point on the scleral surface of the eye and m_i' is defined as point on the insertion needle instantaneously coincident with m_i , Fig. 5. To meet the above constraint, the velocity of m_i' must be equal to the velocity of point m_i in the plane perpendicular to the needle axis:

$$\mathbf{v}_{m_i'\perp} = \mathbf{v}_{m_i\perp} \tag{23}$$

Taking a dot product in the directions, $\hat{\mathbf{x}}_{Q_i}$ and $\hat{\mathbf{y}}_{Q_i}$, yields two independent constraint equations:

$$\hat{\mathbf{x}}_{Q_i}^t\mathbf{v}_{m_i'} = \hat{\mathbf{x}}_{Q_i}^t\mathbf{v}_{m_i} \tag{24}$$

$$\hat{\mathbf{y}}_{Q_i}^t\mathbf{v}_{m_i'} = \hat{\mathbf{y}}_{Q_i}^t\mathbf{v}_{m_i} \tag{25}$$

These constraints can be expressed in terms of the joint angles and eye velocity by relating the velocities of point m_i and m_i' to the robot and eye coordinate systems. The velocity of point m_i' can be related to the velocity of frame $\{Q_i\}$ as follows:

$$\mathbf{v}_{m_i'} = \mathbf{v}_{Q_i} + \boldsymbol{\omega}_{Q_i}\times\overrightarrow{q_im_i} \tag{26}$$

By substituting the twist of frame $\{Q_i\}$, Eq. (26) becomes

$$\mathbf{v}_{m_i'} = [\mathbf{I}_{3\times3}, \mathbf{0}_{3\times3}]\dot{\mathbf{x}}_{Q_i} + \mathbf{E}_i[\mathbf{0}_{3\times3}, \mathbf{I}_{3\times3}]\dot{\mathbf{x}}_{Q_i} \tag{27}$$

where $\mathbf{E}_i = [\overrightarrow{q_im_i}\times]$.

Inserting Eqs. (4) and (1) and writing in terms of the hybrid joint parameters $\dot{\mathbf{q}}_{h_i}$ yields:

$$\mathbf{v}_{m_i'} = \mathbf{F}_i\dot{\mathbf{q}}_{h_i} \tag{28}$$

where $\mathbf{F}_i = \left([\mathbf{I}_{3\times3}, \mathbf{0}_{3\times3}] - \mathbf{E}_i[\mathbf{0}_{3\times3}, \mathbf{I}_{3\times3}]\right)\mathbf{A}_i\mathbf{J}_{P_i}^{-1}[\mathbf{I}_{6\times6}, \mathbf{0}_{6\times2}]$.

An expression for the velocity of the insertion point m_i can be related to the desired eye velocity, similar to the derivation of velocity of point t_i, yielding:

$$\mathbf{v}_{m_i} = \mathbf{M}_i\dot{\mathbf{x}}_e \tag{29}$$

where $\mathbf{M}_i = \left[(-\overrightarrow{em_i})\times\right]$.

Substituting (28) and (29) into (24) and (25) yields the final constraint equations given for the rigid body motion of the eye-robot system:

$$\hat{\mathbf{x}}_{Q_i}^t\mathbf{F}_i\dot{\mathbf{q}}_{h_i} = \hat{\mathbf{x}}_{Q_i}^t\mathbf{M}_i\dot{\mathbf{x}}_e \tag{30}$$

$$\hat{\mathbf{y}}_{Q_i}^t\mathbf{F}_i\dot{\mathbf{q}}_{h_i} = \hat{\mathbf{y}}_{Q_i}^t\mathbf{M}_i\dot{\mathbf{x}}_e \tag{31}$$

Combining these constraints with the twist of the hybrid systems (22) for indices 1 and 2, yields the desired expression of the overall eye-robotic system relating the hybrid robotic joint parameters to the desired EE twists and eye velocity.

$$\begin{bmatrix} \mathbf{K}_1\mathbf{J}_{h_1} & \mathbf{0}_{5x8} \\ \mathbf{0}_{5x8} & \mathbf{K}_2\mathbf{J}_{h_2} \\ \mathbf{G}_1\mathbf{F}_1 & \mathbf{0}_{2x8} \\ \mathbf{0}_{2x8} & \mathbf{G}_2\mathbf{F}_2 \end{bmatrix}\begin{bmatrix} \dot{\mathbf{q}}_{h_1} \\ \dot{\mathbf{q}}_{h_2} \end{bmatrix} = \begin{bmatrix} \mathbf{I}_{5x5} & \mathbf{0}_{5x5} & \mathbf{K}_1\mathbf{D}_1 \\ \mathbf{0}_{5x5} & \mathbf{I}_{5x5} & \mathbf{K}_2\mathbf{D}_2 \\ \mathbf{0}_{2x5} & \mathbf{0}_{2x5} & \mathbf{G}_1\mathbf{M}_1 \\ \mathbf{0}_{2x5} & \mathbf{0}_{2x5} & \mathbf{G}_2\mathbf{M}_2 \end{bmatrix}\begin{bmatrix} \tilde{\dot{\mathbf{x}}}_{g_1/t_1} \\ \tilde{\dot{\mathbf{x}}}_{g_2/t_2} \\ \dot{\mathbf{x}}_e \end{bmatrix} \tag{32}$$

where $\mathbf{G}_i = [\hat{\mathbf{x}}_{Q_i}, \hat{\mathbf{y}}_{Q_i}]^t$.

IV. Simulation Results

To assess and quantify the improvement to the dexterity of the surgeons, we simulated a retinal scan in MATLAB using one branch of the system, provided that the eyeball is fixed in a certain configuration. As derived in Section III, the Jacobian for one arm is a 6×8 matrix, where the first 6 columns corresponds to the Jacobian for the parallel robot,

and the last 2 columns corresponds to the Jacobian for the IODR. To evaluate the impact of the IODR on improving the intra-ocular dexterity, we carried out simulations that compare the dexterity of the robotic arm in Fig. 3 with and without the IODR. For the configuration of the system without the IODR, a straight cannula capable of rotating about its own longitudinal axis was modeled, therefore yielding a 7 DoF robot. The Kinematic Conditioning Index (KCI) was used for dexterity evaluation. The KCI, as defined in [26, 28], is the ratio of the smallest and largest singular value of a Jacobian normalized by a characteristic length. In order to show the change in dexterity for translational and rotational motions, we separated the Jacobian into two submatrices. The upper three rows correspond to translational dexterity, while the lower three rows correspond to rotational dexterity. We separated and normalized the 7 DoF robot Jacobian into translational and rotational submatrices:

$$\mathbf{J}_{7DoF\_t} = [\mathbf{I}_{3\times3}, \mathbf{0}_{3\times3}] \begin{bmatrix} \mathbf{B}_i \mathbf{A}_i \mathbf{J}_{P_i}^{-1}, & \mathbf{0}_{3\times1} \\ & \hat{\mathbf{z}}_{q_i} \end{bmatrix} \begin{bmatrix} \mathbf{I}_{6\times6} & \mathbf{0}_{6\times1} \\ \mathbf{0}_{1\times6} & 1/L_s \end{bmatrix} \quad (33)$$

$$\mathbf{J}_{7DoF\_r} = [\mathbf{0}_{3\times3}, \mathbf{I}_{3\times3}] \begin{bmatrix} \mathbf{B}_i \mathbf{A}_i \mathbf{J}_{P_i}^{-1}, & \mathbf{0}_{3\times1} \\ & \hat{\mathbf{z}}_{q_i} \end{bmatrix} \begin{bmatrix} L_P \mathbf{I}_{6\times6} & \mathbf{0}_{6\times1} \\ \mathbf{0}_{1\times6} & 1 \end{bmatrix} \quad (34)$$

Eqs. (33) and (34) show the normalized sub-Jacobians for the 7 DoF robot, where $\mathbf{J}_{7DoF\_t}$ represents the translational part and $\mathbf{J}_{7DoF\_r}$ represents the rotational part. L_p and L_s are the selected characteristic lengths for the Stewart platform and the IODR respectively, so that L_p is the length of the adjustable locking arm, i.e., 40 mm, and L_s is the bending radius, r , of the pre-shaped NiTi tube.

Similarly, we separated and normalized the Jacobian of the 8 DoF hybrid robot arm as Eqs. (35) and (36), where $\mathbf{J}_{8DoF\_t}$ and $\mathbf{J}_{8DoF\_r}$ represent the translational and rotational sub-Jacobians, respectively.

$$\mathbf{J}_{8DoF\_t} = [\mathbf{I}_{3\times3}, \mathbf{0}_{3\times3}] \mathbf{J}_{h_i} \begin{bmatrix} \mathbf{I}_{6\times6} & \mathbf{0}_{6\times2} \\ \mathbf{0}_{2\times6} & \mathbf{I}_{2\times2}/L_s \end{bmatrix} \quad (35)$$

$$\mathbf{J}_{8DoF\_r} = [\mathbf{0}_{3\times3}, \mathbf{I}_{3\times3}] \mathbf{J}_{h_i} \begin{bmatrix} L_P \mathbf{I}_{6\times6} & \mathbf{0}_{6\times2} \\ \mathbf{0}_{2\times6} & \mathbf{I}_{2\times2} \end{bmatrix} \quad (36)$$

We plotted the KCI over the workspace of ±20º around a chosen center point of the scanning area on the retina. This point is described by the first two w-v-w Euler angles [5π/6, 7π/4] ^{t} as defined in section III-B. The dexterity results of a straight surgical tool manipulated by a 6-DoF parallel robot plus the rotation of the cannula and of the 8-DoF hybrid system were plotted in Fig. 6 and Fig. 7 . In these plots, θ and ϕ represent the variation in the first two w-v-w Euler angles with respect to the center point of the scanning area.

Fig. 6 and Fig. 7 show that the dexterity is significantly improved for both the translational and the rotational motions by the presence of the IODR. Table II shows the percentage of KCI improvement for aforementioned cases.

TABLE II
AVERAGE KCI OF ONE HYBRID ROBOT WITH AND WITHOUT THE IODR.

	Rotary Cannula (no IODR)	With IODR	Improvement
Translational	0.2665	0.3544	32.98%
Rotational	0.3978	0.5851	47.08%

V. CONCLUSION

To improve on the previous ophthalmic surgical robotic assistance works and driven by the clinical need, we presented a novel two-armed slave manipulator aimed at providing a stand-alone tele-manipulation solution for eye microsurgery. This solution provides precise manipulation of surgical instruments inside the eye while manipulating and stabilizing the eye itself under the microscope. Each arm of this robot is equipped with an IODR that provides an additional bending motion inside the eye, therefore improving the current intraocular 4-DoF provided to rigid surgical instruments to 5 DoFs. The kinematic model of the eye and the two robotic arms was presented in a unified approach that incorporates the desired motion between the tools and the retina and the desired motion of the eye itself under the microscope.

Analysis of the dexterity provided by the use of the IODR shows significant improvement for both translational and rotational motions at the distal end of the instrument.

We believe that the proposed approach of a two-armed robot manipulating an organ and simultaneously operating inside this organ is a novel concept that has a clear need in ophthalmic surgery and potential applications in other micro-surgical applications remain to be explored.

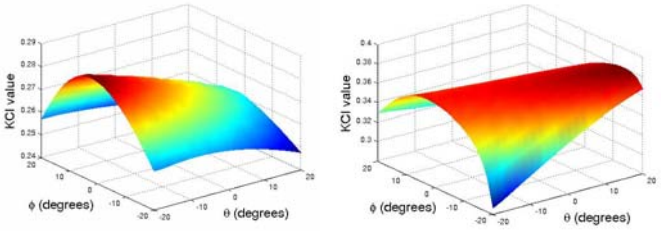

Fig. 6. Translational KCI Plots for One Arm without Distal Dexterity (left) and with Distal Dexterity (right).

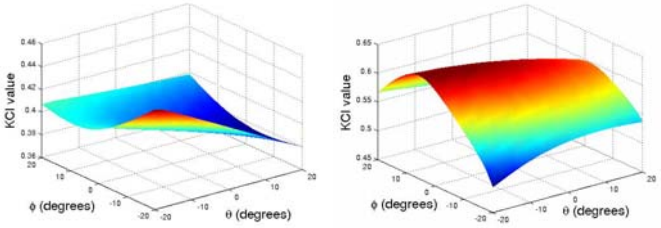

Fig. 7. Rotational KCI Plots for One Arm without Distal Dexterity (left) and with Distal Dexterity (right).

APPENDIX

The 5x1 Euler angle parameterization of the desired ith EE velocity, $\tilde{\dot{\mathbf{x}}}_{g_i/t_i}$, is related in the text to the general twist of the ith robot EE, $\dot{\mathbf{x}}_{g_i/t_i}$, by the degenerate matrix $\mathbf{K}_i$. The matrix

is derived using the relationship found in the literature [29] relating the Cartesian angular velocities to the Euler angle velocities:

$$[\omega_x, \omega_y, \omega_z]^t = \mathbf{R}_i[\dot{\phi}, \dot{\theta}, \dot{\phi}]^t \quad (37)$$

where $\mathbf{R}_i = \begin{bmatrix} 0 & -\sin(\phi_i) & \cos(\phi_i)\sin(\theta_i) \\ 0 & \cos(\phi_i) & \sin(\phi_i)\sin(\theta_i) \\ 1 & 0 & \cos(\theta_i) \end{bmatrix}$.

With the above relationship, the general twist of a system, $\dot{\mathbf{x}}$, can be related to 6x1 Euler angle twist, $[\dot{x}, \dot{y}, \dot{z}, \dot{\phi}, \dot{\theta}, \dot{\phi}]^t$, as follows:

$$[\dot{x}, \dot{y}, \dot{z}, \dot{\phi}, \dot{\theta}, \dot{\phi}]^t = \mathbf{S}_i \dot{\mathbf{x}} \quad (38)$$

where $\mathbf{S}_i = \begin{bmatrix} \mathbf{I} & \mathbf{0} \\ \mathbf{0} & \mathbf{R}_i^{-1} \end{bmatrix}$.

The 5x1 Euler parameterization used in the path planning equation of the text is derived by applying a 5x6 degenerate matrix to the 6x1 Euler angle twist, as follows:

$$\tilde{\dot{\mathbf{x}}} = [\mathbf{I}_{5\times5}, \mathbf{0}_{5\times1}][\dot{x}, \dot{y}, \dot{z}, \dot{\phi}, \dot{\theta}, \dot{\phi}]^t \quad (39)$$

Substituting the relationship between the generalized and the 6x1 Euler angle twist (38) above yields the Matrix $\mathbf{K}_i$ as follows:

$$\tilde{\dot{\mathbf{x}}} = \mathbf{K}_i \dot{\mathbf{x}} \quad (40)$$

where $\mathbf{K}_i = [\mathbf{I}_{5\times5}, \mathbf{0}_{5\times1}]\mathbf{S}_i$.

REFERENCES

[1] S. Charles, "Dexterity Enhancement for Surgery," R. H. Taylor, S. Lavallee, G. C. Burdea, and R. Mosges, Eds. Cambridge, MA: MIT Press, 1996, pp. 467-472.

[2] M. C. Cavusoglu, W. Williams, F. Tendick, and S. Sastry, "Robotics for Telesurgery: Second Generation Berkley/UCSF Laprascopic Telesurgical Workstation and Looking towards the Future Applications," in *39th Allerton Conference on Communication, Control and Computing* Monticello, Italy, 2001, p. Invited Paper.

[3] P. Dario, C. Paggetti, N. Troisfontaine, E. Papa, T. Ciucci, M. C. Carrozza, and M. Marcacci, "A Miniature Steerable End-Effector for Application in an Integrated System for Computer-Assisted Arthroscopy," in *IEEE International Conference on Robotics and Automation*, 1997, pp. 1573-1579.

[4] E. Dombre, M. Michelin, F. Pierrot, P. Poignet, P. Bidaud, G. Morel, T. Ortmaier, D. Salle, N. Zemiti, P. Gravez, M. Karouia, and N. Bonnet, "MARGE Project: Design, Modelling, and Control of Assistive Devices for Minimally Invasive Surgery," in *MICCAI 2004 (7th International Conference on Medical Image Computing and Computer-Assisted Intervention)*, 2004, pp. 1-8.

[5] A. Faraz and S. Payandeh, "Synthesis and Workspace Study of Endoscopic Extenders with Flexible Stem," *ASME Journal of Mechanical Design,* vol. 119, pp. 412-414, 1997.

[6] K. Ikuta, K. Yamamoto, and K. Sasaki, "Development of Remote Microsurgery Robot and New Surgical Procedure for Deep and Narrow Space," in *IEEE International Conference on Robotics and Automation*, 2003, pp. 1103-1108.

[7] M. Mitsuishi, H. Wtanabe, H. Nakanishi, H. Kubota, and Y. IIZUKA, "Dexterity Enhancement for a Tele-micro-surgery System with Multiple Macro-micro Co-located Operation Point Manipulators and Understanding of the Operator's Intention," in *Lecture Notes in Computer Science (LNCS)* vol. 1205, J. Troccaz, E. Grimson, and R. Mosges, Eds.: Springer, 1997, pp. 821-830.

[8] D. Reynaerts, J. Peirs, and H. Van Brussel, "Shape memory micro-actuation for a gastro-intesteinal intervention system," *Sensors and Actuators,* vol. 77, pp. 157-166, 1999.

[9] N. Simaan, R. Taylor, and P. Flint, "High Dexterity Snake-like Robotic Slaves for Minimally Invasive Telesurgery of the Upper Airway," in *MICCAI 2004 (7th International Conference on Medical Image Computing and Computer-Assisted Intervention)*, 2004, pp. 17-24.

[10] N. Simaan, R. Taylor, P. Flint, and A. Hillel, *Minimally Invasive Surgery of the Upper Airways: Addressing the Challenges of Dexterity Enhancement in Confined Spaces* vol. Nova Science Publications, 2005.

[11] H. Yamashita, D. Kim, N. Hata, and T. Dohi, "Multi-Slider Linkage Mechanism for Endoscopic Forceps Manipulator," in *IEEE International Conference on Intelligent Robots and Systems (IROS)*, 2003, pp. 2577-2582.

[12] N. Simaan, R. Taylor, and P. Flint, "A Dexterous System for Laryngeal Surgery - Multi-Backbone Bending Snake-like Slaves for Teleoperated Dexterous Surgical Tool Manipulation," in *IEEE International Conference on Robotics and Automation*, New Orleans, 2004, pp. 351-357.

[13] K. W. Grace, "Kinematic Design of an Ophthalmic Surgery Robot and Feature Extracting Bilateral Manipulation," in *Mechanical Engineering*: Northwestern University, 1995.

[14] H. Das, T. Ohm, C. Boswell, E. Paljug, G. Rodriguez, R. Steele, and E. Barlow, "Telerobotics for Microsurgery," in *18th Annual International Conference of the IEEE Engineering in Medicine and Biology Society*, Amsterdam, 1996, pp. 227-228.

[15] S. Charles, H. Das, T. Ohm, C. Boswell, G. Rodriguez, R. Steele, and D. Istrade, "Dexterity-enhanced telerobotic microsurgery " in *ICAR 1997*, Monterey, CA, USA, 1997, pp. 5-10.

[16] W. T. Ang, P. Khosla, and C. Riviere, "An Intelligent Hand-Held Microsurgical Instrument for Improved Accuracy," in *Proceedings of the 23rd EMBS International Conference*, Istanbul, Turkey, 2001, pp. 25-28.

[17] R. Kumar, P. Berkelman, P. Gupta, A. Barnes, P. S. Jensen, L. L. Whitcomb, and R. H. Taylor, "Preliminary experiments in cooperative human/robot force control for robot assisted microsurgical manipulation," in *International Conference on Robotics and Automation*, San Francisco, CA, USA, 2000, p. 610.

[18] R. Taylor, P. Jensen, L. Whitcomb, A. Barnes, R. Kumar, D. Stoianovici, P. Gupta, Z. Wang, E. deJuan, and L. Kavoussi, "Steady-hand robotic system for microsurgical augmentation," *International Journal of Robotics Research,* vol. 18, p. 1201, 1999.

[19] K. Ikuta, T. Kato, and S. Nagata, "Development and experimental verification of micro active forceps for microsurgery," in *Proceedings of the International Symposium on Micromechatronics and Human Science*, Nagoya, Jpn, 1996, pp. 229-234.

[20] D. Albert and M. Lucarelli, *Clinical Atlas of Procedures in Ophthalmic Surgery*: AMA Press, 2004.

[21] S. Okazawa, R. Ebrahimi, J. Chuang, S. E. Salcudean, and R. Rohling, "Hand-held steerable needle device," *IEEE/ASME Transactions on Mechatronics,* vol. 10, p. 285, 2005.

[22] R. J. Webster, A. M. Okamura, and N. J. Cowan, "Toward Active Cannulas: Miniature Snake-Like Surgical Robots," in *IEEE/RSJ International Conference on Intelligent Robots and Systems (IROS)*, 2006.

[23] A. J. Bron, Tripathi,R.C., Tripathi,B.J. , "Wolff's Anatomy of the Eye and Orbit," vol. 8th Edition. London: Chapman and Hall, 1997.

[24] C. Gosselin, "The optimum design of robotic manipulators using dexterity indices," *Robotics and Autonomous Systems,* vol. 9, pp. 213-226, 1992.

[25] J.-P. Merlet, "Singular Configurations of Parallel Manipulators and Grassmann Geometry," *International Journal of Robotics Research,* vol. 8, pp. 45-56, 1989.

[26] J. Angeles, *Fundamentals of Robotic Mechanical Systems*, 2nd ed.: Springer, 2002.

[27] L.-W. Tsai, *Robot Analysis: The Mechanics of Serial and Parallel Manipulators*: John-Wiley & Sons, INC., 1999.

[28] J.-P. Merlet, "Jacobian, Manipulability, Condition Number, and Accuracy of Parallel Robots," *ASME J. of Mech. Des.,* vol. 128, pp. 199-206, 2006.

[29] Y. Nakamura, *Advanced Robotics Redundancy and Optimization*: Addison-Wesley Publishing Company, 1991.